IEEE Access
Multidisciplinary | Rapid Review | Open Access Journal

Received September 7, 2021, accepted October 5, 2021, date of publication October 8, 2021, date of current version October 15, 2021.

Digital Object Identifier 10.1109/ACCESS.2021.3119042

Unity Proportional Gain Resonant and Gain Scheduled Proportional (PR-P) Controller-Based Variable Perturbation Size Real-Time Adaptive Perturb and Observe (P&O) MPPT Algorithm for PV Systems

CAGFER YANARATES, YIDONG WANG, AND ZHONGFU ZHOU
Electrical and Electronic Engineering Department, Swansea University Bay Campus, Swansea SA1 8EN, U.K.

Corresponding author: Cagfer Yanarates (887912@swansea.ac.uk)

This work was supported in part by the European Regional Development Fund (ERDF) through the Flexis Project.

ABSTRACT In this paper, Proportional Gain Resonant and Gain Scheduled Proportional (PR-P) Controller based variable perturbation size real-time adaptive perturb and observe (P&O) maximum power point tracking (MPPT) algorithm is presented. The proposed control scheme resolved the drawbacks of conventional P&O MPPT method associated with the use of constant perturbation size that leads to poor transient response and high continuous steady-state oscillations. The prime objective of using the PR-P controller is to utilize inherited properties of the signal produced by the controller's resonant path and integrate it to update best estimated perturbation that represents the working principle of extremum seeking control (ESC) to use in P&O algorithm that characterizes the overall system learning-based real time adaptive (RTA). Additionally, utilization of internal dynamics of the PR-P controller overcome the challenges namely, complexity, computational burden, implantation cost and slow tracking performance in association with commonly used soft computing intelligent systems and adaptive control strategies. The proposed control scheme is verified using MATLAB/Simulink by applying comparative analysis with PI controlled conventional P&O MPPT algorithm. Moreover, performance of the proposed control scheme is validated experimentally with the implementation of MATLAB/Simulink/Stateflow on dSPACE Real-time-interface (RTI) 1007 processor board, DS2004 A/D and CP4002 Digital I/O boards. The experimental results and analysis reveal that the proposed control strategy enhanced the tracking speed five times with reduced steady-state oscillations around maximum power point (MPP) and more than 99% energy extracting efficiency.

INDEX TERMS Enhanced adaptive P&O MPPT, extremum seeking control, photovoltaic emulator, proportional resonant controller, state-space averaging, time and frequency domain analysis.

I. INTRODUCTION

Over the last several decades, energy policy in the world has presented a conspicuous tendency of increase in utilization of renewable energy sources for power generation. The underlying reasons of new trend can be summarized as depletion of unsustainable energy resources, environmental considerations, energy supply-demand security, technological advances in renewable energy [1], [2].

The associate editor coordinating the review of this manuscript and approving it for publication was Ton Duc Do.

Photovoltaic (PV) energy has gained wide currency among prevalent renewable energy sources with significant developments in energy conversion and storage technologies. Furthermore, the PV energy systems attracts a great deal of attention owing to considerable advantages such as reliability and long-life, advanced manufacturing process, static and noise-free operations, increasing efficiency, decreasing prices, flexibility of construction and availability of government support and incentives [3], [4]. The evolving requirements and needs in PV energy systems has prompted authorities to do comprehensive studies in this field with

primary motivations of increasing the efficiency, reliability and useful life-span of the PV systems and conversely reducing the cost and space from generation to delivering of the energy [5], [6].

Employing MPPT algorithms is essential in terms of improving energy harvesting efficiency in PV systems since electrical characteristics of PV modules are weather dependent and manifested in the output current and voltage waveforms under variations of irradiance and ambient temperature [7]. A series of recent studies indicated that soft computing intelligent systems such as particle swarm optimization (PSO) [8], fuzzy logic (FL) [9], [10], genetic algorithms (GA) [11], artificial neural networks (ANN) [12], machine learning (ML) [13], differential evolution (DE) [14], ant colony optimization (ACO) [15], artificial bee colony (ABC) [16], grey wolf (GW), firefly (FF) [17] and cuckoo search (CS) [18] have come into widespread use in the development of MPPT techniques for the PV systems as a result of increasing use of hardware-in-the-loop (HIL) and RTI applications. Soft computing intelligent systems, although having higher efficiency in the presence of abrupt and dynamic irradiance and temperature changes, have several evident disadvantages; for instance, complexity, computational burden, implementation cost, slow tracking speed, lacking flexibility, sensitivity of initialization for multi-level optimization [19], [7]. Consequently, many existing studies in the literature have re-visited the conventional MPPT methods such as P&O, hill climbing (HC) and incremental conductance (IC) for further examination to improve [20].

P&O MPPT technique is one of the most common and the simplest algorithms that stands out amongst others with its fast convergence to MPP [21], [22]. However, continuous oscillations around the MPP with respect to the imposed perturbation and production of average MPP value lower than it could be due to large step size are considered as shortcomings of this method [23]. Depending on the perturbation size, the oscillation results in certain amount of power loss and improper choice of the step size leads to poor tracking performance [24].

In this paper, a novel PR-P controller based variable perturbation size real-time adaptive P&O MPPT algorithm is presented. The proposed control scheme resolved the drawbacks of conventional P&O MPPT method associated with the use of constant perturbation size that leads to poor transient response and high continuous steady-state oscillations. The prime objective of using the PR-P controller is to utilize inherited properties of the signal produced by the controller's resonant path and integrate it to update best estimated perturbation that represents the principle of ESC operation to use in P&O algorithm that characterizes the overall system learning-based RTA. Additionally, utilization of internal dynamics of the PR-P controller eliminates the necessity for assistive methods and decreases the number of control system components that overcomes the challenges namely, complexity, computational burden, implantation cost and slow tracking performance in association with commonly used soft computing intelligent systems and adaptive control strategies.

The paper is organized as follows. Section II introduces the overall system control structure with detailed analysis of each unit and discretization of the proposed PR-P controller. Section III is devoted to present the emulated PV panel construction and to derive mathematical model (Transfer function model) of the proposed DC-DC boost converter. together with discussion and comparative analysis of designing and operational principle of the proposed control method. Section IV contains comparative analysis of the proposed PR-P controller and PI controller on the control of the derived model of the boost converter along with the overall system simulation outputs. Section V presents experimental results and discussion.

II. PROPOSED CONTROL STRUCTURE

Block diagram of the control structure is given in Figure 1. The proposed control method is developed by using the properties of PR-P controller, extremum seeking control (ESC) technique and conventional P&O MPPT algorithm together.

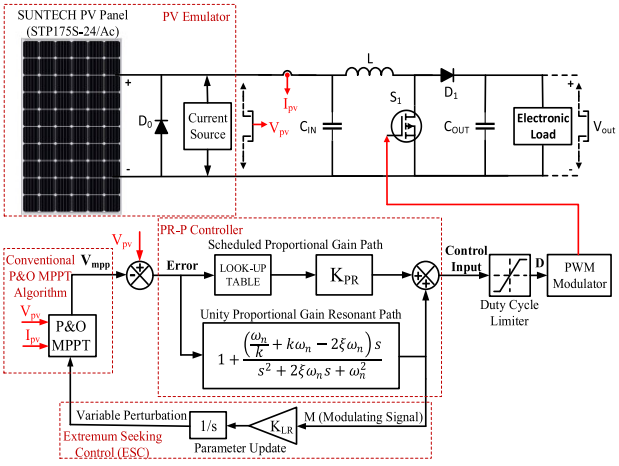

FIGURE 1. Block diagram of the proposed control structure.

In the proposed control structure, PR-P controller is the key component since it performs multiple tasks simultaneously that are error compensation and modulation signal generation from its resonant path as shown in Figure 1. The PR-P controller enables to obtain high gain at any frequency. In this study, it is designed at pulse width modulation (PWM) switching frequency where the signal distortion in the system occurs due to harmonics. Although the ESC is a relatively straightforward controller, it is more complicated due to containing many parameters to be tuned. Modulation signal generation from the unity gain resonant path of the PR-P controller dispenses with the need for using high and low pass filters as well as modulating signal in ESC implementation. Stated in other words, quickly and robustly converging of the system on the optimal solution for perturbation is achieved by utilizing the inherited properties of the PR-P controller.

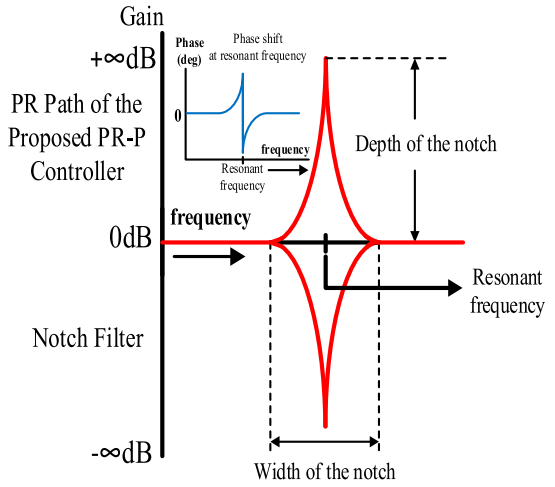

FIGURE 2. Generic frequency response of a notch filter and a PR controller.

A. THE PR-P CONTROLLER DESIGN

The PR controller has become widely used current regulator for grid-connected single-phase inverter systems [25]–[27]. The most important feature of the PR controller is its capability of tracking repeating signals with zero steady-state error by producing high gain at specified frequency.

The PR controller itself is not a method used in DC-to-DC converters but its property that enables control of gain at a specified frequency range is instrumental in developing of the proposed control method. Transfer function of the ideal PR controller is represented by:

$$G_{PR}(s) = K_P + K_I \frac{s}{s^2 + \omega_r^2} \tag{1}$$

where K_P, K_I and ω_r are defined as proportional gain, integral gain, and resonant frequency, respectively.

The problem associated with the use of the ideal PR controller transfer function is that it attains infinite gain at ω_r. The introduced infinite gain leads to an infinity quality factor which cannot be achieved in either analog or digital applications [28]. Stability problems associated with the infinite gain at the resonant frequency are prevented with a non-ideal PR controller which is generated by introducing damping to the ideal transfer function [29], [30]. The non-ideal PR controller transfer function with addition of the bandwidth (ω_c) around the ac resonant frequency (ω_r) is represented by:

$$G_{PR}(s) = K_P + K_I \frac{2\omega_c s}{s^2 + 2\omega_c s + \omega_r^2} \tag{2}$$

The generic frequency response of a notch filter and a PR controller is given in Figure 2. Attaining phase shift at the resonant frequency is one of the key points of the proposed control method. In ESC, this phase shift is a tuning parameter to line up better with the perturbation signal. In the proposed method, the inherited dynamics of the resonant path is used for this purpose that simplifies control strategy.

The design process of the PR controller in the study is based notch filter dynamics and subsequently taking

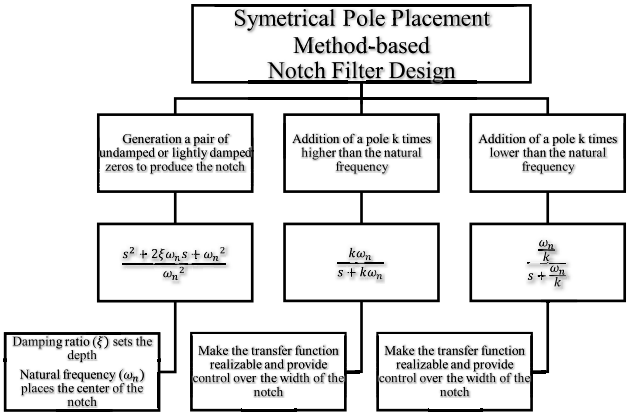

FIGURE 3. Complementary pole placement method-based notch filter design process.

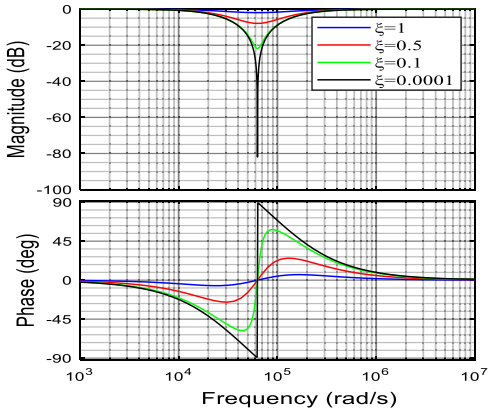

(a) Frequency response with varying ξ.

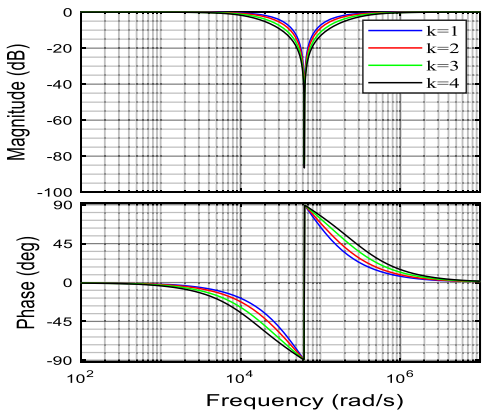

(b) Frequency response with varying k.

FIGURE 4. Phase and magnitude response of the notch filter.

reciprocal of the generated notch filter transfer function at intended frequency [31]. Designing method of the notch filter involving parameters with their functions is given in Figure 3.

The effects of variations in the damping ratio (ξ) and the parameter k on frequency response of the notch characterized by magnitude and phase responses is given in Figure 4. The parameter k is set to adjust the width of the notch, the damping

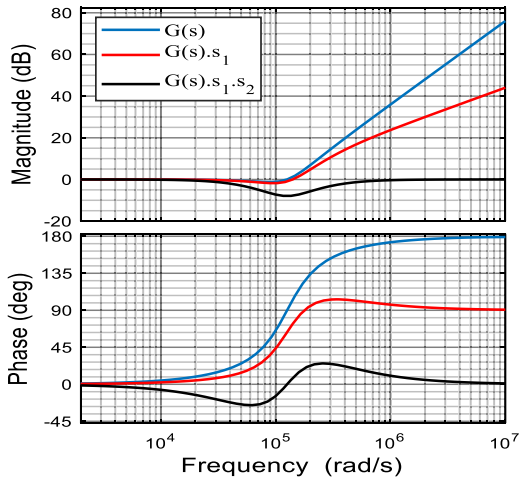

FIGURE 5. The notch filter dynamics-based PR controller.

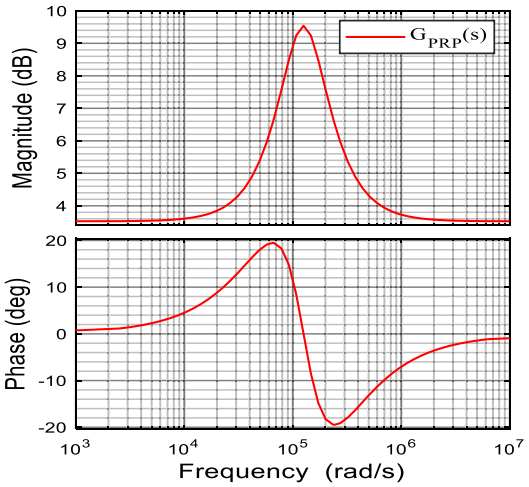

FIGURE 6. Magnitude and phase response of the designed PR-P controller.

ratio (ξ) is set to adjust the depth of the notch and the natural frequency (ω_n) is set to adjust the location of the notch that refers to resonant frequency for the PR path of the proposed PR-P controller.

The variable k will be defined as the ratio of each pole located on both sides of the natural frequency that determines cut-off frequencies of the complementary poles. The parameter k can be adjusted according to the requirement. The larger value of k corresponds with a wider notch, and vice versa. An unrealizable transfer function $G(s)$ generated by locating a pair of zeros with damping ratio of 0.5 at the PWM switching frequency of boost converter which is 20 kHz corresponding to the resonant frequency of the PR path and setting the parameter k value to 2 for the applications is given by:

$$G(s) = \frac{s^2 + 2\xi\omega_n s + \omega_n^2}{\omega_n^2} \tag{3}$$

First pole s_1 with a cut-off frequency k times larger than the natural frequency is given by:

$$s_1 = \frac{k\omega_n}{s + k\omega_n} \tag{4}$$

Second pole s_2 with a cut-off frequency k times smaller than the natural frequency is given by:

$$s_2 = \frac{\frac{\omega_n}{k}}{s + \frac{\omega_n}{k}} \tag{5}$$

Addition of both poles s_1 and s_2 to the transfer function $G(s)$ results in a formation of a second-order band-stop filter whose transfer function $G_{notch}(s)$ is given by:

$$\begin{aligned} G_{notch}(s) &= G(s).s_1.s_2 \\ &= \frac{s^2 + 2\xi\omega_n s + \omega_n^2}{\omega_n^2} \cdot \frac{k\omega_n}{s + k\omega_n} \cdot \frac{\frac{\omega_n}{k}}{s + \frac{\omega_n}{k}} \end{aligned} \tag{6}$$

Figure 5. shows the frequency response of intended notch filter. $G(s)$ is the physically unrealizable transfer function of which order of numerator is greater than denominator given in (3). There is a gain rising at 40 dB/decade since there are two unanswered zeros, thus the high frequency signals are to pass through altered. $G(s).s_1$ shows that addition of a pole with a cut-off frequency that is k times larger than the natural frequency dragged the high frequency magnitude down by 20 dB/decade. $G(s).s_1.s_2$ shows that addition of a complementary pole with a cut-off frequency that is k times smaller than the natural frequency bended down the high frequency magnitude by 20 dB/decade to the zero db.

The transfer function of the resonant path of the proposed PR-P controller $G_{PR}(s)$ is the reciprocal of the notch filter transfer function $G_{notch}(s)$ is presented as:

$$\begin{aligned} G_{PR}(s) &= \frac{1}{G(s).s_1.s_2} \\ &= \frac{\omega_n^2}{s^2 + 2\xi\omega_n s + \omega_n^2} \cdot \frac{s + k\omega_n}{k\omega_n} \cdot \frac{s + \frac{\omega_n}{k}}{\frac{\omega_n}{k}} \end{aligned} \tag{7}$$

$$G_{PR}(s) = \frac{1.579e10s^2 + 4.961e15s + 2.494e20}{1.579e10s^2 + 1.984e15s + 2.494e20} \tag{8}$$

Addition of the proportional gain K_{PR}, ($K_{PR} = 0.5$), to the PR path puts the proposed controller into final form as:

$$\begin{aligned} G_{PRP}(s) &= K_{PR} + G_{PR}(s) \\ &= \frac{2.369e10s^2 + 5.953e15s + 3.741e20}{1.579e10s^2 + 1.984e15s + 2.494e20} \end{aligned} \tag{9}$$

The magnitude and phase responses of the designed PR-P controller is given in Figure 6. The highest gain and phase shift of the proposed PR-P controller occurs at the PWM switching frequency of the boost converter ($\omega_n = 20kHz$). The phase response shows that the phase shift is zero for low and high frequencies.

Unity feedback control structure of the boost converter with the proposed PR-P controller in s-domain from feedback error to control input to the plant is presented as:

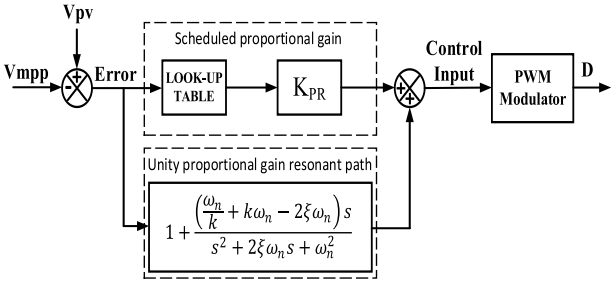

FIGURE 7. Unity feedback control structure of the boost converter with the proposed PR-P controller.

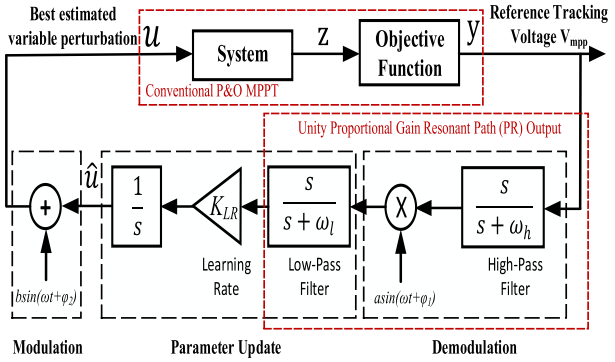

FIGURE 8. The block diagram of extremum seeking control.

B. DISCRETIZATION OF THE PR-P CONTROLLER

In digital control systems, the controller is implemented on a digital computer which means that it will only run and have access to measurements and then command the actuators at specific and discrete times. Transformation from a continuous system to a discrete system causes loss of information which may negatively impact the proposed control system performance. Additionally, discrete systems add delay into the feedback loop which decreases bandwidth of the controller. The bandwidth is very essential parameter as it determines the upper limit on the frequency that the control system can respond. Regarding these challenges, choosing a proposer discretization method is of prima importance.

There are several discretization methods commonly used in control systems, namely, zero-order hold (ZOH), first-order hold (FOH), impulse invariant, bilinear (Tustin) approximation and matched pole-zero method. Bilinear (Tustin's method) approximation is used for the discretization of the proposed PR-P controller. The Main reason of using this method is due to its property of yielding the best frequency-domain match between the continuous-time and discrete systems. The equation employed in the approximation of the z-domain transfer function relating to its continuous form (s-domain) is given as:

$$z = e^{sT_s} \approx \frac{1 + sT_s/2}{1 - sT_s/2} \tag{10}$$

The discretization $G_{PR}(z)$ of a continuous transfer function $G_{PR}(s)$ with sample frequency one order of magnitude higher than the switching frequency ($T_s = 1/10f_{sw}$):

$$G_{PR}(z) = G_{PR}(s'), \quad s' = \frac{2z-1}{T_s z+1}$$
$$G_{PR}(z) = \frac{1.334z^2 - 1.276z + 0.2217}{z^2 - 1.2767z + 0.5553} \tag{11}$$

C. EXTREMUM SEEKING CONTROL (ESC) ALGORITHM

Extremum seeking control (ESC) is an adaptive equation free method of controlling non-linear systems. The operating principle of this method is to add sinusoidal perturbation to the controller and consequently this perturbation allows the algorithm locally to optimize an objective function which is tracking the maximum power point in PV systems. The block diagram of the ESC is given in Figure 8. Unlike optimal control theory method such as linear quadratic regulator (LQR) which requires a linear model of the system and a quadratic objective function to do optimization, ESC and P&O type of algorithms do not require a system model [32]. Furthermore, the optimization is done offline and produces static gains which will stay the same even though the dynamics of the objective system changes over time in LQR. The use of ESC and P&O with the PR-P controller overcome the limitations associates with the use of several optimal control theory methods in PV systems.

ESC algorithm consists of the following stages to tune a parameter value which is generating variable perturbation for the conventional P&O MPPT algorithm that converges quickly to the maximum power point voltage and tracks it efficiently in this study:

- Modulation: The value of the optimization parameter is perturbed with a low-amplitude sinusoidal signal.
- System response: The targeting system being optimized reacts to the parameters perturbations.
- Demodulation: The objection function output signal is multiplied by a sinusoidal signal. The frequency of both modulation and demodulation signals must be the same. A high pass filter is used to remove bias from the objective function output signal. A small phase shift can be implemented to provide better line-up with the perturbation signal.
- Parameter update: The demodulating signal is integrated in this stage to update the parameter value corresponding to state of the integrator. A low-pass

Parameters of the ESC algorithm with their names are given in Table 1.

Execution of the ESC algorithm on the power-voltage (P-V) characteristics curve of a PV module is given in Figure 9.

D. CONVENTIONAL P&O MPPT ALGORITHM

The P&O MPPT approach one of the most basic and widely used algorithms in PV systems which does not require a system model and a quadratic objective function. It can run

TABLE 1. Extremum seeking control parameters.

Name	*Parameter*
Estimated paramater value	$\hat{u}$
Modulated signal	u
Objective function output	y
Forcing frequency	ω
Modulation signal	$bsin(\omega t + \varphi_2)$
Demodulation signal	$bsin(\omega t + \varphi_1)$
Low-pass filter cut-off frequency	ω_l
Higg-pass filter cut-off frequency	ω_h

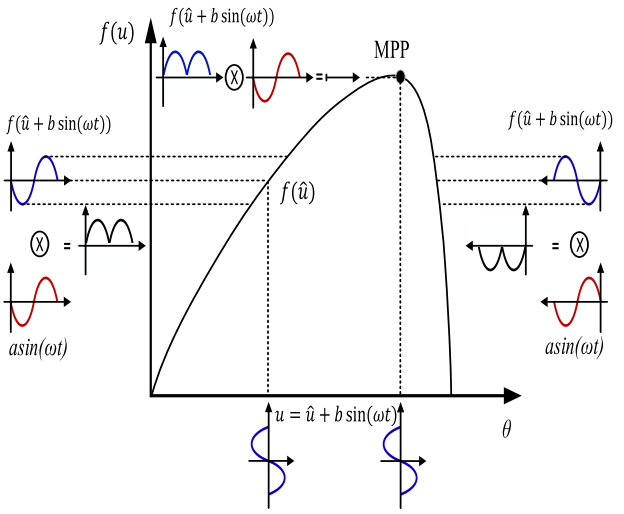

FIGURE 9. Execution of the ESC algorithm on the P-V curve.

real time and adapt to the changing dynamics of the system over time. Operation principle of the algorithm is based on a trial-and-error approach to finding and tracking the MPP.

To compute the power, the approach requires merely measuring the PV array's current and voltage and accordingly perturbing the duty cycle based on a comparison of the initial and present values of the power and voltage until attaining the MPP. Continuous oscillations around the MPP in relation to the imposed perturbation, as well as the development of an average MPP value lower than it could be due to the huge step size, are regarded flaws in this method. The oscillation loses a certain amount of power depending on the size of the perturbation, and improper step size selection leads to poor tracking performance. The flowchart of the algorithm and accordingly its execution on the P-V characteristics curve is given in Figure 10.

III. EMULATED PV PANEL AND STATE-SPACE AVERAGE MODELING OF THE BOOST CONVERTER

A. EMULATED PV PANEL

Variations in irradiance and ambient temperature affect the current generated by the PV module, which is reflected in the output current and voltage waveforms. Since the

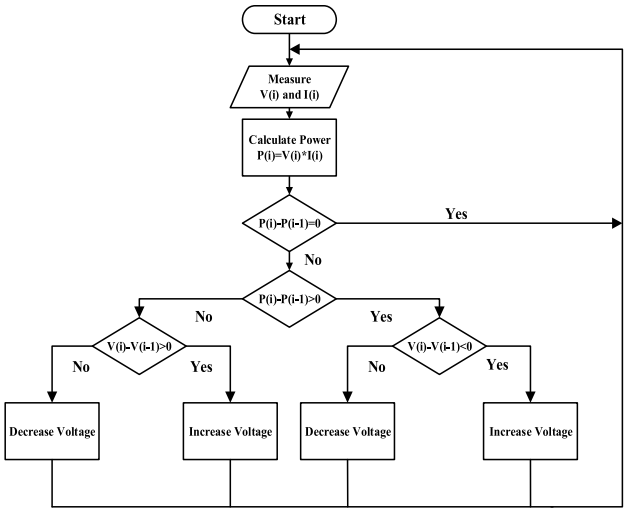

(a) The flowchart of the P&O algorithm.

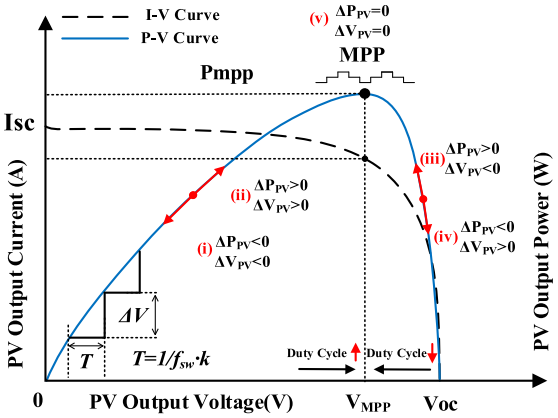

(b) Execution of the P&O algorithm on P-V curve.

FIGURE 10. Perturb and observe (P&O) algorithm.

controlling of these parameters are infeasible for repeatable testing conditions such as MPPT algorithms, inverter control for different operating conditions, testing of charge controller, performance analysis of and comparison of modelled PV panels with the emulator, PV emulating systems which mimic the characteristics of solar panels with fast transient response have become indispensable part of PV applications. Regarding this, an emulated PV panel is constructed by connecting a SUNTECH PV panel (STP175S-24/Ac) whose parameters are given in Table 2. with a DC power supply (ISO-TECH-ISO1603D) that operates in current source mode in parallel. Insignificant amount of current generated by the panel due to the indoor conditions is ignored.

The DC power supply is used to inject an external current that represents the amount of the irradiance to simulate the current generated by the solar panel. Varying irradiance condition current generation is achieved by manually altering the output current (injected current) of the DC power supply. The equivalent circuit of the emulated PV panel is shown

TABLE 2. The emulated PV module (STP175S-24/Ac) parameters.

Parameter	Value
Maximum Power (W)	174.24
Open Circuit Voltage V_{OC} (V)	44.2
Voltage at Maximum Power Point V_{MPP} (V)	35.2
Temperature Coefficient of V_{OC} (%/deg.C)	-0.36699
Cells per Module (Ncell)	72
Short-circuit Current I_{SC} (A)	5.2
Current at Maximum Power Point I_{MPP} (A)	4.95
Temperature Coefficient of I_{SC} (%/deg.C)	0.042

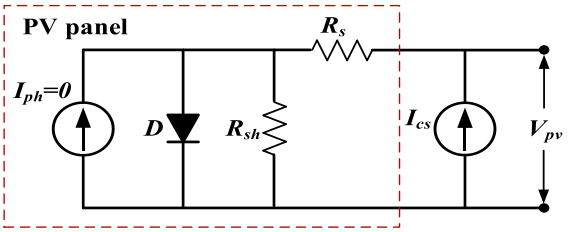

FIGURE 11. The equivalent circuit of the emulated PV panel.

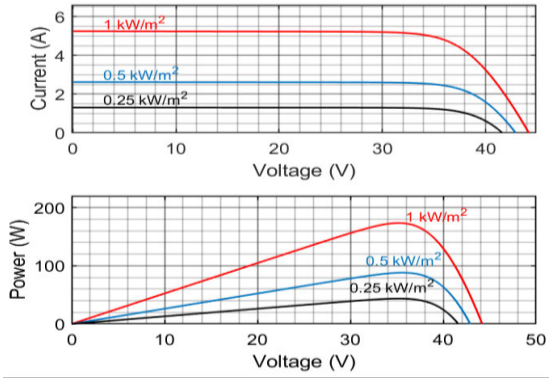

FIGURE 12. Characteristics curves of the emulated PV module (STP175S-24/Ac).

in Figure 11. where Ics represents the external excitation current.

Figure 12. shows the characteristics current-voltage (I-V) and power-voltage (P-V) curves of the emulated PV panel for varying irradiance values used in the simulations.

B. STATE-SPACE AVERAGE MODELING OF THE BOOST CONVERTER

A control system manages the behaviour of plants for the regulations to meet the requirements using control loops. A plant consists of process and actuator, and it can be represented with a set of mathematical equations (mathematical model). Commonly used mathematical models in the control systems are differential equation model, transfer function model and state-space model. Main purpose of using one of these mathematical models is to simplify control system design and analysis in both time and frequency domains. The classical control theory introduces closed-loop control (feedback) to overcome limitations associates with the use of open-loop control. Primary advantages of the closed-loop controllers over open-loop controllers are disturbance rejection, better performance with parameters' uncertainties of the model, capability in the stabilization of unstable processes, sensitivity reduction to variations of model parameters and enhancement of reference tracking.

In this paper, transfer function model of the intended boost converter is used to design and analyse the proposed PR-P controller to improve important dynamic properties of the plant such as stability, speed of response, steady-state error, oscillations which constitute the transient and the steady-state response of the system. Intended boost converter transfer function is derived by using dynamic (AC small signal) state-space averaging technique. This process includes taking the Laplace Transform (with zero initial condition) of both the state and output equations in the state-space model of the boost converter [33]. The flowchart of the state-space averaging technique is given in Figure 13.

State-Space Average Method is one of the developed techniques to obtain the transfer function of the plant, analyse properties and behaviours of the switch mode power supplies (SMPS) [34], [35]. Providing a substantial insight and its simplicity for both derivation and implementation has made the method a very useful and convenient tool in the applications of power electronics devices [34], [36]. There are two states determined according to ON-and-OFF the transistor in the circuit, so SMPS circuit analysis consists of two topologies. Description of operating range (intervals) for each state has been made by commonly used conversions and notations as the following:

$$\begin{aligned} d &\equiv \textit{duty ratio} \\ d' &\equiv 1 - d \\ T_{sw} &\equiv \textit{switching period} \end{aligned} \tag{12}$$

A linear-time-invariant (LTI) system model in the state-space form can be represented as [37]:

$$\begin{aligned} \dot{x} &= Ax + Bu \\ y &= Cx + Du \end{aligned} \tag{13}$$

Each state of the boost converter can be described as a set of linear-time-invariant differential equations. The state and output equation for the ON-state during the interval of dT_{sw} is:

$$\begin{aligned} \dot{x} &= A_1 x + B_1 v_{in} \\ y_1 &= C_1 x \end{aligned} \tag{14}$$

The state and output equation for the OFF-state during the interval of $d'T_{sw}$ is:

$$\begin{aligned} \dot{x} &= A_2 x + B_2 v_{in} \\ y_2 &= C_2 x \end{aligned} \tag{15}$$

The elements of the state vector x are inductor currents and capacitor voltages as inductor and capacitor are the

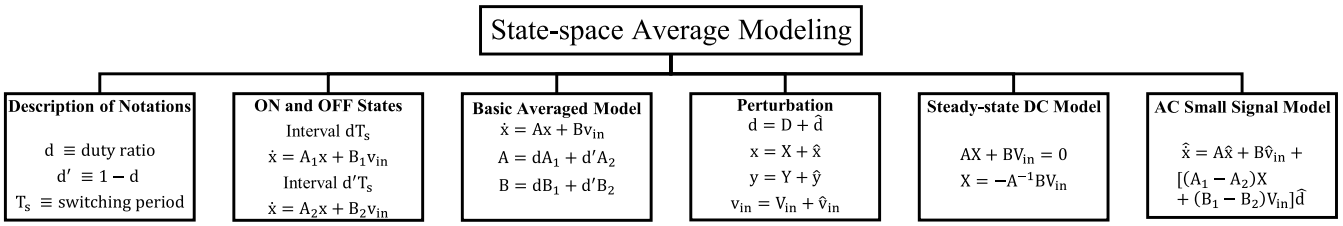

FIGURE 13. Flowchart of state-space average modeling of switch mode power supply.

only energy storage components of the boost converter. To obtain a single continuous state-space equation (single matrix differential equation) (14) and (15) must be combined in a sense of averaging the system, input and output matrices to result in A, B and C matrices. The averaging process purely depends on the duty ratio (d) and it is executed as:

$$\begin{aligned} A &= dA_1 + d'A_2 \\ B &= dB_1 + d'B_2 \\ C &= dC_1 + d'C_2 \end{aligned} \tag{16}$$

The vector block diagram for a linear-time-invariant system in terms of state-space dynamics is in given in Figure 14. and the average state-space equation of the system is given in (17).

$$\begin{aligned} \dot{x} &= Ax + Bv_{in} \\ y &= Cx \end{aligned} \tag{17}$$

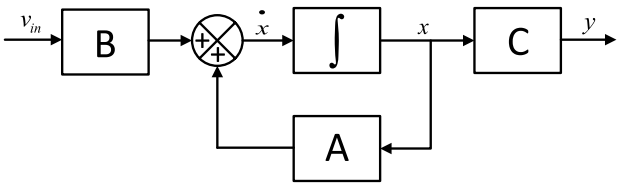

FIGURE 14. Linear system state-space vector diagram.

Equation (17) describes the averaged behaviour of the boost converter, and it basically removes ripples of the inductor current and capacitor voltage that are the inherent property of the state variables. One of the significant points to note here is that the system matrix A and the input matrix B may be duty ratio dependent, which leads to the conclusion that the averaged equation may be non-linear regarding the duty ratio (d). The purpose of using state-space model of the boost converter is to generate an equivalent circuit model and carrying out the analysis of the system around a linearization point by perturbing the averaged equation about this operation point. Small signal variation with the steady state values is represented as:

$$\begin{aligned} d &= D + \hat{d} \\ x &= X + \hat{x} \\ y &= Y + \hat{y} \\ v_{in} &= V_{in} + \hat{v}_{in} \end{aligned} \tag{18}$$

The capitalized quantities in (18) represent the steady state values and the carets are small perturbations. The perturbation is performed by making substitution (18) into (17) and the expanding of the new state-space equation is obtained as the following:

$$\begin{aligned} \dot{X} + \dot{x} = &\left[\left(D + \hat{d}\right)A_1 + \left(1 - D - \hat{d}\right)A_2\right]\left(X + \hat{x}\right) \\ &+ \left[\left(D + \hat{d}\right)B_1 + \left(1 - D - \hat{d}\right)B_2\right]\left(V_{in} + \hat{v}_{in}\right) \\ Y + \hat{y} = &\left[\left(D + \hat{d}\right)C_1 + \left(1 - D - \hat{d}\right)C_2\right]\left(X + \hat{x}\right) \end{aligned} \tag{19}$$

The equation for steady-state operating point when the small signal perturbations are zero is:

$$\begin{aligned} 0 &= AX + BV_{in} \\ Y &= CX \end{aligned} \tag{20}$$

Discarding of the second order small signal variation terms in (19) results in AC small signal (dynamic) model of the system as following:

$$\begin{aligned} \dot{\hat{x}} &= A\hat{x} + B\hat{v}_{in} + [(A_1 - A_2)X + (B_1 - B_2)V_{in}]\hat{d} \\ \hat{y} &= C\hat{x} + (C_1 - C_2)X\hat{d} \end{aligned} \tag{21}$$

A, B and C matrices in (21) are:

$$\begin{aligned} A &= DA_1 + D'A_2 \\ B &= DB_1 + D'B_2 \\ C &= DC_1 + D'C_2 \end{aligned} \tag{22}$$

Setting $\hat{v}_{in}$= 0 produces the response to the variation of the duty factor and (21) transforms into the following equation:

$$\begin{aligned} \dot{\hat{x}} &= A\hat{x} + [(A_1 - A_2)X + (B_1 - B_2)V_{in}]\hat{d} \\ \hat{y} &= C\hat{x} + (C_1 - C_2)X\hat{d} \end{aligned} \tag{23}$$

The simplified representation of the state equation in (23) is:

$$\dot{\hat{x}} = A\hat{x} + F\hat{d} \tag{24}$$

Variation of state variables to the duty factor can be easily solved by application of the Laplace Transform as the following:

$$\frac{\hat{x}}{\hat{d}} = [sI - A]^{-1}F \tag{25}$$

In (25), notation I stands for the unit matrix that is the same size of the system matrix A and $[sI - A]^{-1}$ is the inverse of the matrix $[sI - A]$.

Thus far, the state-space modelling of the DC-to-DC switch mode power converter is represented in terms of small-signal and low-frequency behaviour by deriving an equivalent linear circuit description comprising of averaging, perturbation, and linearization process.

In the experimental set-up, the emulated solar panel is connected to a step-up DC-DC converter (boost converter) and supplies power to the electronic load. The boost converter consists of an inductor, power switch MOSFET, power diode and output capacitor, as shown in the Figure 15. The required PV terminal voltage which refers to the maximum power point voltage is achieved by regulating the duty cycle of the PWM signal with the proposed control method.

Design parameters of the boost converter used for in this work given in Table 3.

TABLE 3. Design parameters of the boost converter.

Parameter	Value
Input voltage(V_{dc})	44.2 V
Switching frequency (f_{sw})	20 kHz
Inductance (L)	100 µH
Output capacitance (C_{out})	440 µF
Constant voltage load (V_{out})	70 V

Implementation of (12-25) and the design parameters for the boost converter in terms of duty ratio to output voltage yields the transfer function in s-domain as:

$$G_{boost}(s) = \frac{V_{out}(s)}{d(s)} = \frac{\left[\frac{-V_{dc}}{RC_{out}(D-1)^2}\right]s + \frac{V_{dc}}{C_{out}L}}{s^2 + \left(\frac{1}{RC_{out}}\right)s + \frac{(D-1)^2}{C_{out}L}} \quad (26)$$

$$G_{boost}(s) = \frac{-0.00442s + 34.53}{3.13e-08s^2 + 3.91e-05s + 0.31} \quad (27)$$

Input-output voltage relationship of steady-steady in (20) is represented as:

$$\frac{V_{out}}{V_{dc}} = \frac{1}{1-D} \quad (28)$$

The transfer function of the boost converter in terms of duty ratio to input voltage can be derived by substituting (28) into (26) as:

$$G_{boost}(s) = \frac{V_{dc}(s)}{d(s)} = \frac{1}{(1-D)} \frac{\left[\frac{-V_{dc}}{RC_{out}(D-1)^2}\right]s + \frac{V_{dc}}{C_{out}L}}{s^2 + \left(\frac{1}{RC_{out}}\right)s + \frac{(D-1)^2}{C_{out}L}} \quad (29)$$

$$G_{boost}(s) = \frac{-0.0071s + 55.25}{3.13e-08s^2 + 3.91e-05s + 0.31} \quad (30)$$

IV. COMPARATIVE ANALYSIS OF THE PR-P AND PI CONTROLLERS

Control systems are often designed to improve the system characteristics such as stability, speed of response, steady-state error, or prevent oscillations after obtaining an appropriate model of the system. Mathematical model of a system is used in the analysing of the system to predict its respond in both the time and frequency domains. Time domain analysis of a system represents how the state of a dynamic system changes in time while being subjected to a particular input. In other respects, frequency domain analysis of a system comprises of magnitude and phase differences between sinusoidal input and steady-state output of the system as a function of frequency.

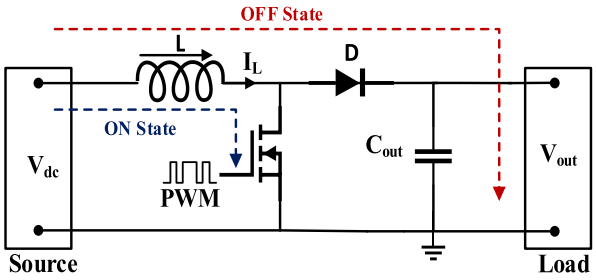

FIGURE 15. Circuit diagram of a boost converter.

Performance assessment of the proposed PR-P control structure is done by using comparative analysis evalution method with widely used PI control structure. Both controllers are designed by considering the SMPS stability criteria given in Table 4.

TABLE 4. Switch mode power supply stability criteria.

Parameters	Value
Crossover (cutoff frequency)	Between the range of $1/10^{th}$ to $1/8^{th}$ of switching frequency
Phase Margin	Greater than 45 degree
Gain Margin	Greater than 10 dB
The slope of the gain curve at the crossover frequency	≈-20 db/decade

Closed-loop step response comparison plot of the derived transfer function of the boost converter controlled with the proposed PR-P controller and PI controller is:

Step response characteristics of the boost converter in terms of open-loop and closed-loop is given in Table 5. Time domain analysis of the system regarding transient and steady-state characteristics indicates that similar performance outcomes are achieved with the proposed PR-P controller for a step change.

SMPS output signals display repetitive sinusoidal-like behaviours inherently due to its nature therefore time delays must be considered during the process of building a controller for a dynamical system to analyse its performance. Time delays exist in two variations named signal distorting and non-distorting transport delays. Signal distorting delay stands for phase lag in which each frequency is delayed by a different amount of time and non-distorting delay in which the entire signal is postponed by the same amount of time.

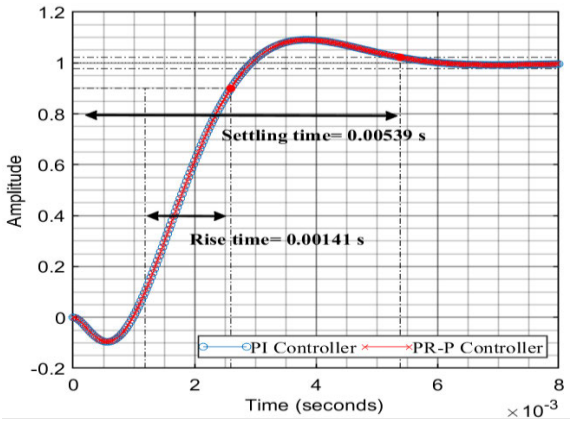

FIGURE 16. Closed-loop step response of the controllers.

TABLE 5. Time domain analysis of the boost converter control.

Step Reponse Characteristics	Open-loop	Closed-loop PI Control	Closed-loop PR-P Control
Rise Time	6.4e-04	0.0014	0.0014
Settling Time	0.0014	0.0054	0.0054
Settling Minimum	102.54	0.9084	0.9093
Settling Maximum	115.64	1.0909	1.0906
Overshoot	2.20	9.0851	9.0638
Undershoot	45.36	9.6256	9.6287
Peak	115.65	1.0909	1.0906
Peak Time	0.002	0.0039	0.0039

The main components cause time delays in a feedback system are sensors, actuators, controller, and the process itself.

Step-response of the feedback loop combined with a sinusoidal interference whose amplitude is 0.2 and frequency is 10 kHz in the presence of internal delay is given in Figure 17.

Step-response of the feedback loop combined with the same sinusoidal interference in the presence of both internal delay which is unintentional accruing due to the process itself and feedback signal transport delay is given in Figure 18.

A properly designed controller that is perfectly tuned to the model may still be under the risk of reduced performance on the real system. Straightforward approach to overcome this problem is to add margin (time delay) into the design. Regarding this issue, a consistent system must be designed in such a way to ensure that the stability is exceeded in a certain amount instead of just meeting the desired performance so any deviations on the system dynamics will not affect the requirements. In this sense, the proposed PR-P controller has achieved superior enhanced performance in comparison to PI controller as shown in Figure 18.

The output voltage of all DC/DC converters is a function of the duty ratio. To prevent control loop instabilities and ensure proper operation of the boost converter requires considering about the duty cycle limitations in practical applications. The estimated duty ratio (D) for the boost

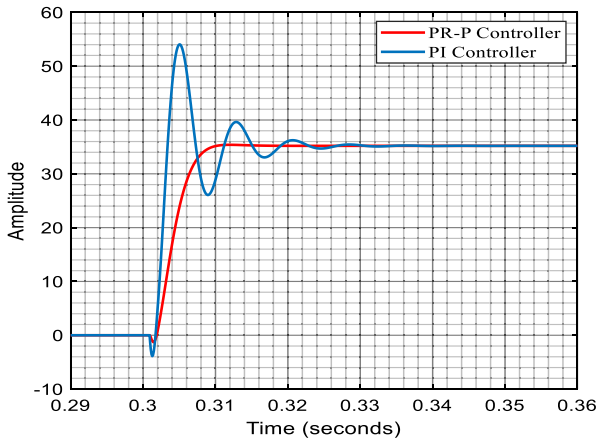

FIGURE 17. Closed-loop step response with internal time delay.

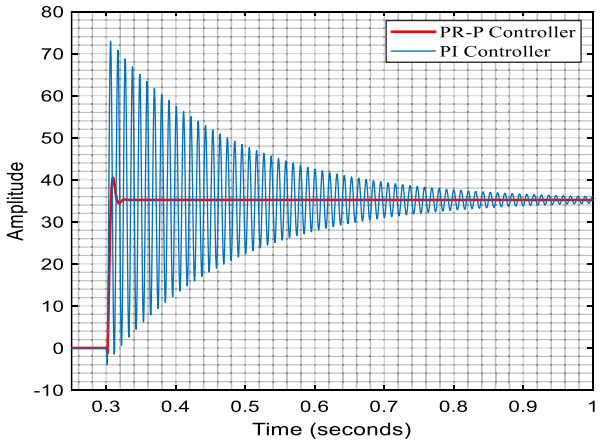

FIGURE 18. Closed-loop step response with internal and signal transport time delays.

converter can be calculated as:

$$D = 1 - \frac{V_{in}\eta}{V_{out}} \tag{31}$$

where V_{in}, V_{out} and η are input voltage to regulator, output voltage of the regulator and efficiency, respectively. Properties of the boost converter components such as parasitic resistance in the inductor and MOSFET, the voltage drop of the diode set an upper limit on the duty ratio and therefore the output voltage. The general representation of practical boost converters' boost ratio and duty cycle relationship is given in Figure 19. [38], [39].

The approximate maximum duty ratio for both synchronous and non-synchronous boost converters is calculated can be calculated by considering given load current I_{out}, input voltage V_{in} and component resistances as:

$$D_{MAX} \cong \frac{V_{in} - I_{out}(R_1 + R_2 + 2R_L)}{V_{in} + I_{out}(R_1 - R_2)} \tag{32}$$

where R_1, R_2 and R_L are resistance of MOSFET switch, resistance of synchronous MOSFET (if applicable) and resistance of inductor, respectively. In this paper, for the purpose of simplicity the minimum (D_{min}), nominal (D_{nom})

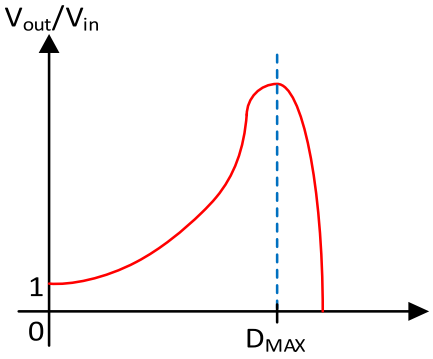

FIGURE 19. Boost ratio & duty cycle relationship.

and maximum (D_{max}) duty cycle values are calculated as:

$$D_{min} = \frac{V_{out} + V_D - V_{in(\max)}}{V_{out} + V_D}$$
$$D_{nom} = \frac{V_{out} + V_D - V_{in(\text{nom})}}{V_{out} + V_D}$$
$$D_{max} = \frac{V_{out} + V_D - V_{in(\min)}}{V_{out} + V_D} \quad (33)$$

where constant output voltage (V_{out}) with the value of 70 V, maximum input voltage ($V_{in(\max)}$) with the value of 44.2 which is the open circuit voltage of the emulated PV panel SUNTECH (STP175S-24/Ac), nominal input voltage ($V_{in(\text{nom})}$) with the value of 35.2 which is the maximum power point voltage of the emulated PV panel at 1000 W/m^2 and 25 deg. C, minimum input voltage ($V_{in(\min)}$) with value of 10 V and the forward voltage (V_D) of the output diode with the value of 0.5 V. According to these parameters calculated duty cycle corresponds with the 10-90% range in which many controllers operate properly.

In addition to the duty cycle, another primary component of the PWM control of the SMPS is the switching frequency. The PWM signal generation is a method to for creating digital pulses to control analog circuits and the simplest way to generate a PWM signal is the intersective method which requires only a sawtooth or triangular waveform. The control input or duty cycle generated from the controller is used to track the reference input. In this application, the PI and the proposed control scheme outputs are compared with a sawtooth waveform to track the desired V_{mpp}. The frequency of the sawtooth is 20 kHz which is the switching frequency of the boost converter. The PWM signals for both the PI and the proposed control scheme are given in Figure 20. While the proposed control scheme PWM generation remains constants, the conventional P&O MPPT with PI controller PWM generation presents non-constant switching frequency [40]. The advantage of fixed switching frequency in SMPS applications is that any switching noise arising can be predicted, thus facilitates the filtering process. Alternatively stated, the constant switching frequency makes the design of passive filters simpler. Furthermore, it gains more control over physical size of components, electrical characteristics, frequency response and power losses of the boost converter.

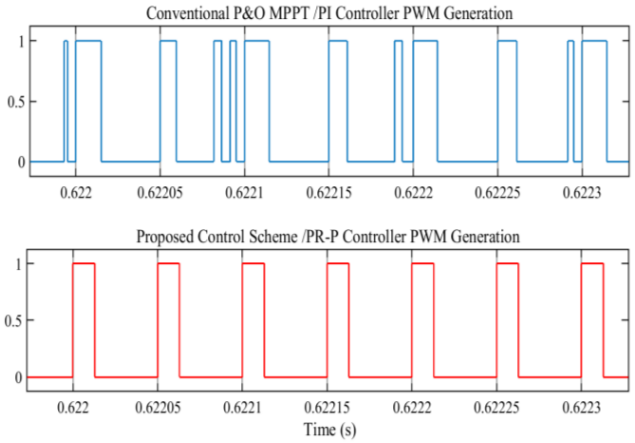

FIGURE 20. Partial section views of PWM signals for the conventional PI and the proposed PR-P control methods in steady-state.

Figure 20. shows that conventional P&O MPPT algorithm with PI controller PWM generation signal has the period of 27.891 μs and 35.854 kHz in a steady-state partial section, although frequency of the sawtooth modulation signal is 20 kHz. However, the proposed control scheme with PR-P controller PWM generation signal has the same fixed frequency as the modulating signal.

A fixed perturbation size P&O MPPT with a PI controller and the proposed unity proportional gain resonant and gain scheduled proportional (PR-P) controller based variable perturbation size real-time adaptive P&O MPPT simulation results are generated in MATLAB/Simulink. The fixed perturbation step size is set at $\Delta V = 0.5$ with a frequency of 200 Hz corresponding to perturbation period of $\Delta T = 5$ ms and irradiance variations are applied with sudden step changes of 1000 W/m^2, 250 W/m^2 (severe shading condition) and 500 W/m^2.

Figure 21. shows the voltage waveforms under determined varying irradiance. The proposed control strategy shows enhanced tracking performance 5 times faster than conventional method. Additionally, the steady-state oscillations around MPP is reduced significantly with the proposed control scheme.

Figure 22. shows the current waveforms generated under defined conditions. The current outputs verified the improved MPPT performance regarding the tracking speed and reduced oscillations.

Figure 23. shows PV output powers for the PI controlled fixed perturbation P&O MPPT algorithm and the proposed control scheme with the PR-P controller. Approximately 5 times enhancement in the tracking speed and less oscillation in steady-state are observed clearly with the proposed control method.

Table 6. shows the efficiency and tracking performance comparison of conventional fixed perturbation size P&O MPPT with a PI controller and the proposed control scheme with PR-P controller under varying irradiance values considering the emulated PV panel SUNTECH (STP175S-24/Ac) Datasheet Values.

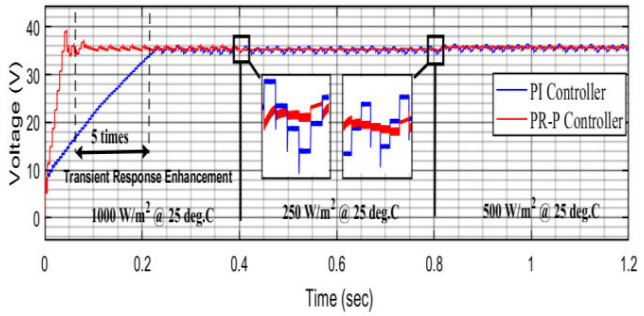

FIGURE 21. Comparison of PV maximum power point voltage (V_{mpp}) tracking performance of conventional and proposed control methods.

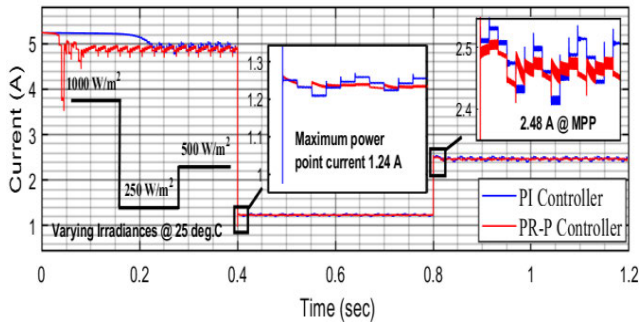

FIGURE 22. Comparison of PV current of conventional and proposed control methods.

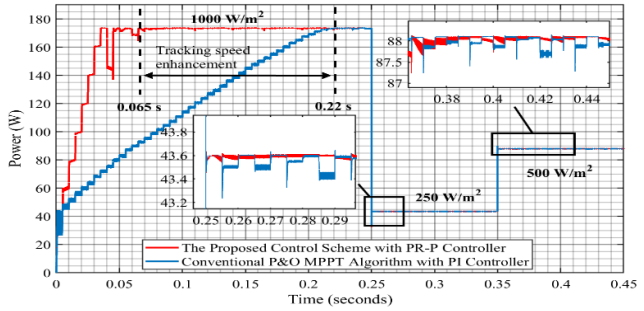

FIGURE 23. PV output powers of conventional and proposed control methods.

V. EXPERIMENTAL RESULTS AND DISCUSSIONS

The block diagram of the experimental setup configuration for testing the proposed MPPT algorithm is given in Figure 24. The overall system consists of the emulated PV panel, the DC-DC boost converter, electronic load for constant DC voltage output, dSPACE real-time Interface (RTI) hardware-in-the-loop (HIL) control panels (RTI 1007 processor board, DS2004 A/D and CP4002 Digital I/O boards).

Test bench of the experiment is given in Figure 25. The emulated 175 W commercial SUNTECH PV panel (STP175S-24/Ac) connected with a 360 W DC power supply (ISO-TECH-ISO1603D) in parallel to create real environment PV characteristics was built as a power supply to the electronic load through the DC-DC boost converter. The terminal voltage of the emulated PV panel is controlled by the boost converter.

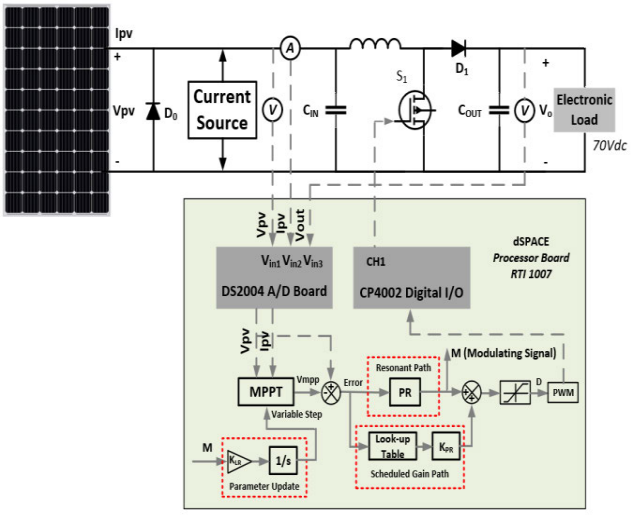

FIGURE 24. Experimental setup configuration for testing the proposed MPPT algorithm.

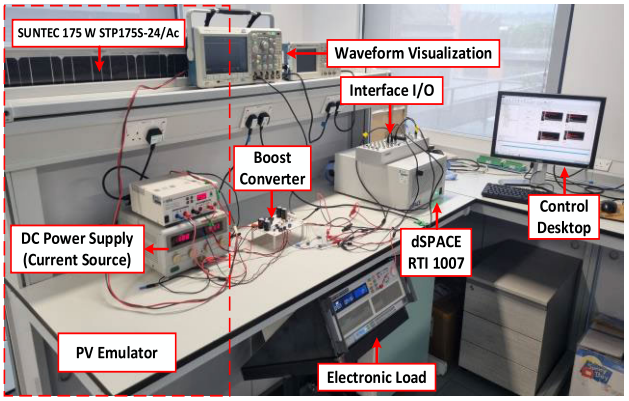

FIGURE 25. Test bench of the overall system.

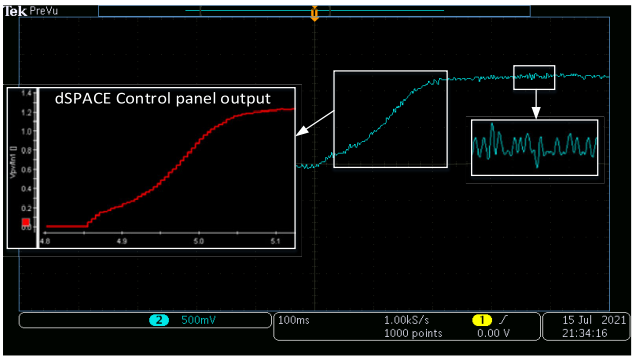

FIGURE 26. PI controlled conventional fixed perturbation step size P&O MPPT algorithm PV voltage.

The proposed MPPT method developed by using MATLAB/Simulink was implemented via dSPACE rapid control prototyping. The RTI block of the Modular Hardware/DS2004 High-speed A/D was used to convert the measured terminal current Ipv and terminal voltage Vpv as shown in Figure 24.

The converted Ipv and Vpv were then implemented in the MPPT algorithm. Due to the limitation in the range of -10 V

TABLE 6. Efficiency and tracking performance comparison of conventional P&O MPPT with a PI controller and the proposed PR-P control scheme.

Irradiance (W/m^2)	SUNTECH (STP175S-24/Ac) Datasheet Values		Conventional P&O MPPT with PI Controller				The Proposed Control Scheme with PR-P Controller			
	Maximum Power Point Voltage (V_{mpp})	Maximum Power (W)	Measured Voltage (V)	Measured Power (W)	Efficiency (η%)	Tracking Speed (s)	Measured Voltage (V)	Measured Power (W)	Efficiency (η%)	Tracking Speed (s)
1000	35.2	174.2	35.44	169.5	97.3	0.22	35.4	170.05	97.6	0.07
750	35.55	131.5	36.07	127.2	96.73	0.25	35.79	128.3	97.56	0.05
500	35.57	88.1	35.76	86.01	97.62	0.26	35.68	87.01	98.76	0.06
250	35.43	43.59	35.35	41.5	95.2	0.27	35.39	42.5	97.49	0.075

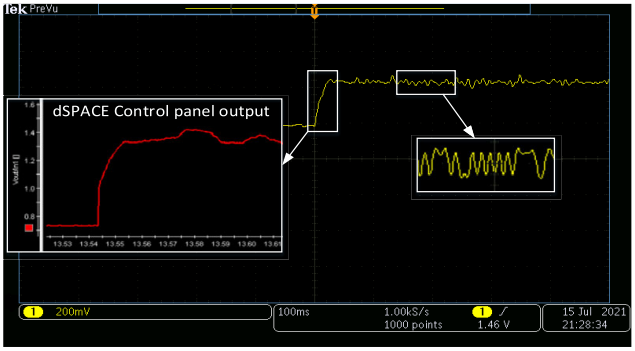

FIGURE 27. PR-P controller based variable perturbation size real-time adaptive P&O MPPT algorithm PV voltage.

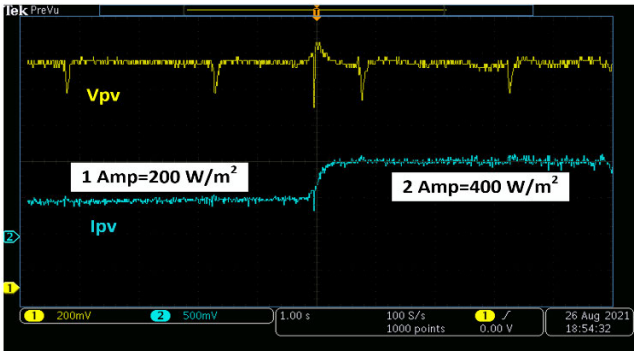

FIGURE 28. PI controlled conventional fixed perturbation step size P&O MPPT algorithm PV voltage for varying irradiance values.

to +10 V of dSPACE Analogue to Digital (A/D) channel, the measured terminal outputs were scaled down. Vpv and Ipv were scaled down by a constant factor of 28 and 2.6, respectively. Regulated duty cycle in the simulink to achieve required terminal voltage was used to generate the PWM signal for running the boost converter. For this purpose, generated digital PWM signal was implemented using dSPACE MATLAB/Simulink PC-based simulation platform Modular Hardware/DS4002 Timing and Digital I/O Board.

Conventional fixed perturbation step size PI controlled P&O MPPT algorithm experimental test result is given in Figure 26.

The proposed unity proportional gain and gain scheduled proportional (PR-P) controller based variable perturbation size real-time adaptive P&O MPPT algorithm experimental test result is given in Figure 27.

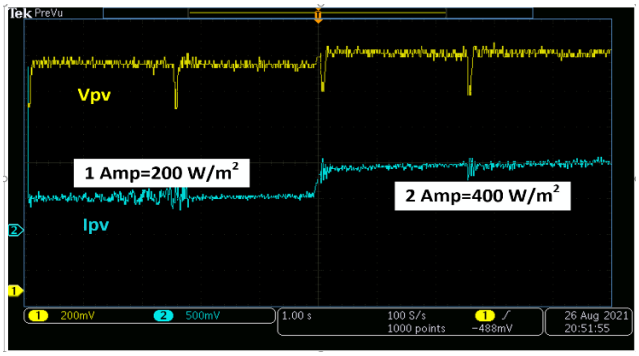

FIGURE 29. PR-P controller based variable perturbation size real-time adaptive P&O MPPT algorithm PV voltage for varying irradiance values.

The measured values in Figure 26. and 27. represent both transient and steady-state responses in terms of terminal voltage of the boost converter for constant current of 1 Amp which stands for approximately 200 w/m^2 irradiance since the maximum power point current of the emulated PV panel is 4.95 at 1000 W/m^2 and 25 deg. C.

Conventional fixed perturbation step size PI controlled P&O MPPT algorithm experimental test result for varying irradiance values is given in Figure 28.

The proposed unity proportional gain and gain scheduled proportional (PR-P) controller based variable perturbation size real-time adaptive P&O MPPT algorithm experimental test result for varying irradiance values is given in Figure 29.

Experimental results are in accordance with the simulation outcomes and both experimental results and analysis reveal that the proposed control strategy enhanced the tracking speed with reduced steady-state oscillations around maximum power point (MPP).

VI. CONCLUSION

This paper has presented Proportional Gain Resonant and Gain Scheduled Proportional (PR-P) Controller based variable perturbation size real-time adaptive perturb and observe (P&O) maximum power point tracking (MPPT) algorithm to overcome the limitations associated with conventional fixed step size PI controlled P&O MPPT algorithm. Moreover,

an alternative unprecedented design process based on changing notch filter dynamics with placement of the complementary poles around the boost converter switching frequency for the PR-P controller is implemented.

The proposed control scheme resolved the drawbacks of conventional P&O MPPT method associated with the use of constant perturbation size that leads to poor transient response and high continuous steady-state oscillations.

The prime objective of using the PR-P controller is to utilize inherited properties of the signal produced by the controller's resonant path and integrate it to update best estimated perturbation (ESC model-free adaptive control technique) to use in P&O algorithm that characterizes the overall system learning-based real time adaptive (RTA). Additionally, utilization of internal dynamics of the PR-P controller overcome the challenges namely, complexity, computational burden, implantation cost and slow tracking performance in association with commonly used soft computing intelligent systems and adaptive control strategies. Although the most common use of proportional-resonant (PR) controllers is in DC/AC applications, the results demonstrated that properties of the PR controllers can be utilized effectively in DC/DC systems.

The proposed control scheme is verified using MATLAB/Simulink by applying comparative analysis with PI controlled conventional P&O MPPT algorithm. Moreover, performance of the proposed control scheme is validated experimentally with the implementation of MATLAB/Simulink/Stateflow on dSPACE Real-time-interface (RTI) 1007 processor board, DS2004 A/D and CP4002 Digital I/O boards. The experimental results and analysis reveal that the proposed control strategy enhanced the tracking speed five times with reduced steady-state oscillations around maximum power point (MPP) and more than 99% energy extracting efficiency.

REFERENCES

[1] R. Ayop and C. W. Tan, "A comprehensive review on photovoltaic emulator," *Renew. Sustain. Energy Rev.*, vol. 80, pp. 430–452, Dec. 2017.

[2] S. Seyam, I. Dincer, and M. Agelin-Chaab, "Development of a clean power plant integrated with a solar farm for a sustainable community," *Energy Convers. Manage.*, vol. 225, Dec. 2020, Art. no. 113434.

[3] W. Xiao, *Photovoltaic Power Systems: Modeling, Design, and Control*, 1st ed. Hoboken, NJ, USA: Wiley, 2017.

[4] G. Price, *Renewable Power and Energy*, 1st ed. New York, NY, USA: Momentum Press, 2018.

[5] B. Carrera and K. Kim, "Comparison analysis of machine learning techniques for photovoltaic prediction using weather sensor data," Tech. Rep., 2020.

[6] L.-L. Li, S.-Y. Wen, M.-L. Tseng, and C.-S. Wang, "Renewable energy prediction: A novel short-term prediction model of photovoltaic output power," *J. Cleaner Prod.*, vol. 228, pp. 359–375, Aug. 2019.

[7] J. Ahmed, S. Member, and Z. Salam, "An improved method to predict the position of maximum power point during partial shading for PV arrays," Tech. Rep., Dec. 2015.

[8] Z. Zhu and G. Liu, "MPPT control method for photovoltaic system based on particle swarm optimization and bacterial foraging algorithm multi-peaks," *Energies*, vol. 4, no. 1, pp. 45–49, 2018.

[9] J. Macaulay, "A fuzzy logical-based variable step size P&O MPPT algorithm for photovoltaic system," *Energies*, vol. 11, no. 6, p. 1340, 2018.

[10] G. Bayrak and D. Ghaderi, "An improved step-up converter with a developed real-time fuzzy-based MPPT controller for PV-based residential applications," *Int. Trans. Electr. Energy Syst.*, vol. 29, no. 12, pp. 1–20, Dec. 2019.

[11] P. Kumar, G. Jain, and D. K. Palwalia, "Genetic algorithm based maximum power tracking in solar power generation," in *Proc. Int. Conf. Power Adv. Control Eng. (ICPACE)*, Aug. 2015, pp. 1–6.

[12] K. Punitha, D. Devaraj, and S. Sakthivel, "Artificial neural network based modified incremental conductance algorithm for maximum power point tracking in photovoltaic system under partial shading conditions," *Energy*, vol. 62, pp. 330–340, Dec. 2013.

[13] M. S. Nkambule, A. N. Hasan, A. Ali, J. Hong, and Z. W. Geem, "Comprehensive evaluation of machine learning MPPT algorithms for a PV system under different weather conditions," *J. Electr. Eng. Technol.*, vol. 16, no. 1, pp. 411–427, Jan. 2021.

[14] M. Seyedmahmoudian, R. Rahmani, S. Mekhilef, A. M. T. Oo, A. Stojcevski, T. K. Soon, and A. S. Ghandhari, "Simulation and hardware implementation of new maximum power point tracking technique for partially shaded PV system using hybrid DEPSO method," *IEEE Trans. Sustain. Energy*, vol. 6, no. 3, pp. 850–862, Jul. 2015.

[15] S. Kinattingal, S. P. Simon, and P. S. Rao, "MPPT in PV systems using ant colony optimisation with dwindling population," *IET Renew. Power Gener.*, vol. 14, no. 7, pp. 1105–1112, 2020.

[16] C. González-castaño, C. Restrepo, S. Kouro, S. Member, and J. Rodríguez, "MPPT algorithm based on artificial bee colony for PV system," Tech. Rep., 2021.

[17] S. Conditions, "An immucne firefly algorithm for tracking the maximum power point of PV array under partial," Tech. Rep., 2019.

[18] J. Ahmed and Z. Salam, "A maximum power point tracking (MPPT) for PV system using cuckoo search with partial shading capability," *Appl. Energy*, vol. 119, pp. 118–130, Apr. 2014.

[19] K. K. Thyagharajan and T. Vignesh, "Soft computing techniques for land use and land cover monitoring with multispectral remote sensing images: A review," *Arch. Comput. Methods Eng.*, vol. 26, no. 2, pp. 275–301, Apr. 2019.

[20] A. Amir, A. Amir, J. Selvaraj, N. A. Rahim, and A. M. Abusorrah, "Conventional and modified MPPT techniques with direct control and dual scaled adaptive step-size," *Sol. Energy*, vol. 157, pp. 1017–1031, Nov. 2017.

[21] R. B. Bollipo, S. Mikkili, and P. K. Bonthagorla, "Critical review on PV MPPT techniques: Classical, intelligent and optimisation," *IET Renew. Power Gener.*, vol. 14, no. 9, pp. 1433–1452, 2020.

[22] A. Ba, C. O. Ehssein, M. E. M. O. M. Mahmoud, O. Hamdoun, and A. Elhassen, "Comparative study of different DC/DC power converter for optimal PV system using MPPT (P&O) method," *Appl. Sol. Energy*, vol. 54, no. 4, pp. 235–245, Jul. 2018.

[23] P. Motsoeneng, J. Bamukunde, and S. Chowdhury, "Comparison of perturb & observe and Hill climbing MPPT schemes for PV plant under cloud cover and varying load," in *Proc. 10th Int. Renew. Energy Congr. (IREC)*, Mar. 2019, pp. 1–6.

[24] Z. Zhou, P. M. Holland, and P. Igic, "MPPT algorithm test on a photovoltaic emulating system constructed by a DC power supply and an indoor solar panel," *Energy Convers. Manage.*, vol. 85, pp. 460–469, Sep. 2014.

[25] T.-K. Vu and S.-J. Seong, "Comparison of PI and PR controller based current control schemes for single-phase grid-connected PV inverter," *J. Korea Academia-Ind. Cooperation Soc.*, vol. 11, no. 8, pp. 2968–2974, Aug. 2010.

[26] F. Blaabjerg, R. Teodorescu, M. Liserre, and A. V. Timbus, "Overview of control and grid synchronization for distributed power generation systems," *IEEE Trans. Ind. Electron.*, vol. 53, no. 5, pp. 1398–1409, Oct. 2006.

[27] M. Ciobotaru, R. Teodorescu, and F. Blaabjerg, "Control of single-stage single-phase PV inverter," in *Proc. Eur. Conf. Power Electron. Appl.*, Sep. 2006, p. 10.

[28] C. Khomsi, M. Bouzid, K. Jelassi, and G. Champenois, "Harmonic current conpensation in a single-phase grid connected photovoltaic system sypplying nonlinear load," in *Proc. 9th Int. Renew. Energy Congr. (IREC)*, Mar. 2018, pp. 1–6.

[29] M. Parvez, M. F. M. Elias, and N. A. Rahim, "Performance analysis of PR current controller for single-phase inverters," in *Proc. 4th IET Clean Energy Technol. Conf. (CEAT)*, 2016, pp. 1–8.

[30] D. Zammit, C. S. Staines, M. Apap, and J. Licari, "Design of PR current control with selective harmonic compensators using Matlab," *J. Electr. Syst. Inf. Technol.*, vol. 4, no. 3, pp. 347–358, Dec. 2017.

[31] C. Yanarates and Z. Zhou, "Symmetrical pole placement method-based unity proportional gain resonant and gain scheduled proportional (PR-P) controller with harmonic compensator for single phase grid-connected PV inverters," *IEEE Access*, vol. 9, pp. 93165–93181, 2021.
[32] S. M. Fatemi, M. S. Shadlu, and A. Talebkhah, "A new method for maximum power point tracking in solar PV systems by combining extremum seeking method (ESM) and model predictive control (MPC)," in *Proc. 11th Power Electron., Drive Syst., Technol. Conf. (PEDSTC)*, Feb. 2020, pp. 5–9.
[33] R. Zaitsu, "Voltage mode boost converter small signal control loop analysis using the TPS61030," Texas Instrum., Dallas, TX, USA, Appl. Rep., 2007.
[34] W. M. Polivka, P. R. K. Chetty, and R. D. Middlebrook, "State-space average modelling of converters with parasitics and storage-time modulation," in *Proc. IEEE Power Electron. Spec. Conf.*, Jun. 1980, pp. 119–143.
[35] P. Azer and A. Emadi, "Generalized state space average model for multi-phase interleaved buck, boost and buck-boost DC-DC converters: Transient, steady-state and switching dynamics," *IEEE Access*, vol. 8, pp. 77735–77745, 2020.
[36] G. Suman, B. V. S. P. Kumar, M. S. Kumar, B. C. Babu, and K. R. Subhashini, "Modeling, analysis and design of synchronous buck converter using state space averaging technique for PV energy system," in *Proc. Int. Symp. Electron. Syst. Design (ISED)*, Dec. 2012, pp. 281–285.
[37] D. Rowell. (Oct. 2002). *State-Space Representation of LTI Systems*. [Online]. Available: http://web.mit.edu/2.14/www/Handouts/StateSpace.pdf
[38] Texas Instruments. (2015). *Working With Boost Converters*. [Online]. Available: http://www.ti.com/lit/an/snva731/snva731.pdf,Ed
[39] V. Michal, "Dynamic duty-cycle limitation of the boost DC/DC converter allowing maximal output power operations," in *Proc. Int. Conf. Appl. Electron. (AE)*, Sep. 2016, pp. 177–182.
[40] H. Xie and E. Guo, "How the switching frequency affects the performance of a buck converter," Tech. Rep., 2019, pp. 1–8.

CAGFER YANARATES was born in April 1986. He received the M.Sc. degree in power engineering and sustainable energy FHEQ7 Taught Masters/PGDip/PGCert from Swansea University, in 2017, where he is currently pursuing the Ph.D. degree with the Electrical and Electronic Engineering Department. He is mainly engaged in applications of power electronics converters in photovoltaics systems and their control.

YIDONG WANG was born in 1995. He received the Bachelor of Mechanical Engineering, in 2018, and the master's degree in power engineering and sustainable energy, in 2019. He is currently pursuing the Ph.D. degree with the Electrical and Electronic Engineering Department, Swansea University. His research interests include power conversion in renewable energy systems and the application of power electronic converter.

ZHONGFU ZHOU received the Ph.D. degree from the University of Sussex, Brighton, U.K., in 2004. He joined the College of Engineering, Swansea University, in 2004, as a Research Officer, and promoted as a Lecturer in power electronics, in July 2016. His research interests include active rectifier, active power filter, and power electronics applications for renewable energy systems and automotive. Since 2010, he has been a member of the International Electrotechnical Commission (IEC), where he has advised on the international standard (IEC TS 62600-30) on electrical power quality requirements for wave, tidal, and other water current energy converters.